

# EMF Mitigation via 5G and 6G MAC Scheduling

Silvio Mandelli, Lorenzo Maggi, Bill Zheng, Christophe Grangeat, Azra Zejnilagic  
Nokia. E-mail: silvio.mandelli@nokia-bell-labs.com

**Abstract**—High antenna directivity allows for high throughput transmission but also increases the exposure to electromagnetic field (EMF) of the end-users. Health regulations impose limitations on the incident power density, that generate a negative impact on network performance.

In this work we focus at the slot-by-slot operations of a cellular MAC scheduler to constrain the short-term EMF exposure upon real-time resource allocation, minimizing the impacts on network performance. We assume that the long-term EMF exposure is controlled by a proper outer-loop technique, that is not the object of this paper. Due to the minimal computational complexity allowed in MAC scheduling, existing solutions allowing practical implementation are few and focused at sub-optimal approaches curbing radio resource allocation.

Our contribution is the derivation of a computationally efficient water-filling solution to allocate power and - then - resources, with a feasible integration of the necessary algorithms in the operations of a 5G MAC scheduler. We finally evaluate our proposal versus the prior art approaches with system level simulations with realistic modeling of physical and MAC level cellular procedures. We conclude that our proposal can control EMF with considerable less impact on network performance, making it a standout candidate for 5G and future 6G MAC scheduler implementations.

**Index Terms**—EMF, RF exposure, EIRP, MAC Scheduling, Power Control.

## I. INTRODUCTION

The high beam directivity characterizing the deployment of fifth generation (5G) cellular networks has sparked concerns regarding potential health risks associated with electromagnetic field (EMF) exposure. However, regulators and the research community have long been committed to thoroughly understanding and addressing any health implications of EMF exposure through continuous regulation and oversight efforts.

The guidelines by the International Commission on Non-Ionizing Radiation Protection (ICNIRP) [1] specify the EMF exposure limits, depending on the operating radio frequency and enforced on the average power density over a sliding time window ranging from 1 to 30 minutes [1], [2]. Such limits can also be defined country-wise.

Ensuring the effective enforcement of such limits while minimizing the impact on the network performance will become increasingly challenging in sixth generation (6G) Multiple Inputs Multiple Outputs (MIMO) deployments where hundreds or thousands antenna elements, hence even higher beam gains than in 5G, are expected [3].

By adopting a conservative approach, one can ensure that EMF constraints are met even in the worst case scenario where users consistently find themselves in the direction of maximum beam gain. This translates to limiting the Effective Isotropic Radiated Power (EIRP) of the radiating antenna array.

Arguably, imposing real-time constraints on EIRP in cellular networks is no easy task, due to the scheduler complexity and the tight computation latency constraint. Existing approaches [4], [5] propose power control procedures limiting the usable bandwidth; [6] optimizes precoding for MIMO systems under the assumption of full channel knowledge. However, this assumption is unfeasible in reality as it would require heavy inter-working between physical and Medium Access Control (MAC) layer. Finally, it has been shown that imposing EIRP constraints affects network performance [7], highlighting the importance of designing algorithms that minimize the performance degradation while being implementable in MAC layer real-time procedures.

**Our contribution.** We consider the framework illustrated in Fig. 1, where an “outer-loop” mechanism operates on a slow time scale, monitoring the average EIRP over a sliding window of a few minutes, as prescribed by ICNIRP. Such mechanism sets the EIRP budget for the next “period” which encompasses the next few hundred of slots. The design of the outer-loop mechanism is not the focus of this paper and can be found, e.g., in [8]. In this paper we focus on the “inner-loop” aspect depicted in Fig. 1, which enforces the EIRP budget in real-time via MAC scheduling operations. Initially, the subset of User Equipments (UEs) eligible for transmission in the current slot is selected as described, e.g., in [9]. Then, the EIRP is controlled by allocating Physical Resource Blocks (PRBs), power and Modulation and Coding Scheme (MCS) *fairly* across UEs. Our proposal comprises two subroutines: the first spreads the EIRP budget across slots within the same period, to accommodate traffic bursts while avoiding budget depletion before the period ends. The second subroutine performs a *fair* allocation across the UEs while fulfilling the constraint on the per-slot EIRP budget.

Prior art [4], [5] proposed constraining resources solely in the frequency - hence PRB - domain to limit EIRP. Instead, we propose dynamically adjusting the user MCS and power to maximize the global UE throughput fairness while adhering to an EIRP constraint. The concept of reducing MCS and power while spreading the transmission across more radio time and frequency resources was already introduced in [10], [11]. Yet, constraints on EIRP were not considered since the primary focus was mitigating interference in non-full buffer scenarios.

Our intuition suggests that, to control EIRP, reducing power similarly to the approach in [10], [11] should be preferred over reducing bandwidth. This reasoning stems directly from the classic Shannon formula: reducing bandwidth leads to a linear decrease in both rate and EIRP, while decreasing power results in a *logarithmic* reduction in rate. These effects tend

to coincide in the low SINR regime. Therefore, we expect power-based EIRP control solutions to drastically outperform bandwidth based approaches, if properly implemented. As a side-product, overall network interference will be reduced, as demonstrated in [10], [11].

We evaluate our proposal in a highly realistic 3rd Generation Partnership Project (3GPP) calibrated simulation setup, with a full physical and MAC implementation of a MIMO cellular scenario. The results enable us to draw conclusions regarding the potential architecture and algorithms for deployment in a MAC scheduler of a g-Node B (gNB) in cellular networks to control EIRP with minimal impact on system performance.

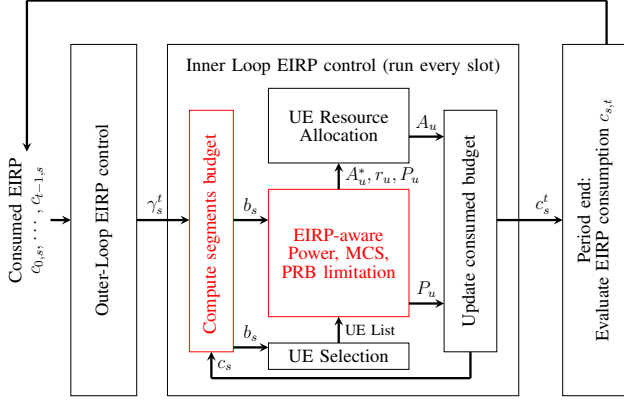


Fig. 1: Block diagram of EIRP control operations considered in this work. Slot index  $k$  has been omitted in inner-loop operations for readability. The main focus of our work concerns the red blocks, while the other parts are either legacy MAC scheduling operations in the inner-loop, or outer-loop operations discussed in [8]

## II. EMF EXPOSURE MODEL

We address the downlink (DL) scheduling problem of allocating PRBs and power to users while mitigating the human exposure to EMF according to the health regulations imposed by the ICNIRP.

We first introduce some notation. We let  $A_{u,k}$  and  $P_{u,k}$  be the number of allocated PRBs and the transmit power per PRB for user  $u$  in slot  $k$ , respectively. We denote by  $\beta_{u,k}$  the beam serving user  $u$  in slot  $k$  and we call  $G_{u,k}(\phi, \theta)$  the antenna gain in azimuth/elevation direction  $(\phi, \theta)$  when beam  $\beta_{u,k}$  is used. The set of *active* UEs, i.e., the UEs with DL data in the buffer, is  $\mathcal{U}_k$ .

The EIRP emitted by a radiating antenna array in the azimuth/elevation direction  $(\phi, \theta)$  in slot  $k$  writes:

$$\text{EIRP}_k(\phi, \theta) := \sum_{u \in \mathcal{U}_k} A_{u,k} P_{u,k} G_{u,k}(\phi, \theta). \quad (1)$$

The power density  $D$  measured at distance  $R$  from the antenna in the direction  $(\phi, \theta)$  is proportional to the EIRP, and equals  $D = \frac{\text{EIRP}(\phi, \theta)}{4\pi R^2}$ . ICNIRP imposes health-based limits on  $D$  [1], which can be translated into an upper bound  $\bar{C}$  on the average EIRP, depending on the statistical distribution of the distance of humans from the antenna [7]. Depending on the presence and type of human activities present in

the cell (schools, hospitals, etc.), different limits may need to be imposed in different directions. To account for this, we partition the set of all azimuth/elevation angles, defined with respect to the radiating antenna, into a set of segments *segments*  $\mathcal{S}$ , and assign a specific EIRP limit  $\bar{C}_s$  to each segment  $s \in \mathcal{S}$ . We then define the EIRP *consumption*  $c_{k,s}$  as the maximum EIRP in segment  $s$ :

$$c_{k,s} := \max_{(\phi, \theta) \in s} \text{EIRP}_k(\phi, \theta). \quad (2)$$

We call *period*  $t$  a set of  $K \geq 1$  consecutive slots starting from  $k_0^t$ , and we define  $c_s^t := \sum_{k=k_0^t}^{k_0^t+K-1} c_{k,s}$  the sum of EIRP consumption over period  $t$ . To fulfill the ICNIRP health regulations we impose that the average EIRP consumption over every sliding window of  $W$  consecutive periods does not exceed  $\bar{C}_s$ , for each segment  $s$ :

$$\frac{1}{W} \sum_{i=0}^{W-1} c_s^{t-i} \leq \bar{C}_s, \quad \forall t, s \in \mathcal{S}. \quad (3)$$

## III. POWER CONTROL FOR EMF EXPOSURE MITIGATION

As illustrated in Fig. 1, an outer-loop algorithm computes the limit  $\gamma_s^t$  on the EIRP consumption in period  $t$ , such that

$$0 \leq c_s^t \leq \gamma_s^t, \quad \forall t, s \in \mathcal{S}. \quad (4)$$

The design of the outer-loop algorithm is not the focus of this paper and is discussed, e.g., in [8]. Then, we consider  $\gamma_s^t$  as a predefined input for each  $s, t$ . In this paper we study how to enforce the EIRP cap (4) on a per-slot and on a per-user basis via a so-called *inner-loop* control mechanism within DL MAC scheduler operations depicted in Fig. 1.

Without loss of generality we consider  $k_0^t = 1$ . We then split our problem into two sub-problems that we solve separately.

- 1) **Per-slot EIRP constraint.** For each segment  $s$  and in each period  $t$ , it must hold that  $\sum_{k=1}^K c_{k,s} \leq \gamma_s^t$ . We smooth out the EIRP consumption over time by computing an upper limit - or *slot budget* -  $b_{k,s}$  for  $c_{k,s}$ , for each slot  $k$  and segment  $s$ .
- 2) **Power allocation.** At slot  $k$ , we allocate power fairly across UEs by ensuring  $c_{k,s} \leq b_{k,s}$ .

For simplicity of notation, we hereafter drop the dependence of variables on period  $t$ .

### A. Per-slot EIRP constraint design

Let us fix the segment  $s$ . At the beginning of each slot  $k = 1, \dots, K$ , given the past consumption  $c_{1,s}, \dots, c_{k-1,s}$ , we must cap the EIRP consumption for the upcoming slot to a value  $b_{k,s}$ . We propose to inject a portion  $(1 - \epsilon_s)$  of the period's budget  $\gamma_s$  at slot  $k = 0$  and spread the remainder by injecting  $\epsilon_s \gamma_s / K$  at each slot, with  $0 \leq \epsilon_s \leq 1$ . Therefore, the available slot budget at slot  $k$  is

$$b_{k,s} = \max \left( \left( 1 - \epsilon_s \frac{K-k}{K} \right) \gamma_s - \sum_{i=1}^k c_{i,k}, 0 \right). \quad (5)$$

The difficulty in designing the portion  $\epsilon_s$  resides in the fact that future user requests are unknown. On the one hand, we

want to avoid to greedily deplete the budget early on in the period with  $\epsilon_s$  close to zero, which would lead to empty slots later on. On the other hand, we want to refrain from introducing unnecessarily delay by curbing consumption in an overly conservative manner with  $\epsilon_s$  close to one.

Similarly, we would like to avoid the possible excessively low slot budget as computed in (5). Therefore, the slot budget can be lower bounded by  $\rho_s^* c_s^*$ , where  $c_s^*$  is the maximum EIRP that can be radiated in the segment  $s$  in one slot on all available PRBs and full power and maximum beam gain, and  $0 < \rho_s^* c_s^* < \gamma_s/K$ .

Optionally, we propose to start curbing EIRP once the slot budget is below a certain guard threshold  $b_s^*$ , controlling EIRP emission before the slot budget gets too low. Therefore, we also study the following slot budget refinement

$$b'_{k,s} = c_s^* \exp(\ln(\rho_s^*) \max(1 - b_{k,s}/b_s^*, 0)). \quad (6)$$

### B. Power Limiting (PL) techniques

We now show how to enforce the EIRP constraint  $b_{k,s}$  on segment  $s$  by allocating power to active UEs in a *fair* manner. We assume that  $A_{u,k}$  PRBs have been pre-allocated to each active UE  $u \in \mathcal{U}_k$  as a function of—amongst others—the amount of bits present in the buffer for each UE, the selected MCS and the corresponding rate  $m_u, r_u$ , respectively. In our preferred implementation, this is performed via the method described in [11], which downgrades the UEs' MCS and reduces the power accordingly, hence increasing the required PRB allocation, but without exceeding the PRBs available in the current slot. As a result, the transmit power and resulting interference in neighbouring cells are reduced.

**Two simplifying approximations.** Since power allocation must be decided at every slot, computational complexity is a bottleneck. To simplify the problem we first approximate that each beam  $\beta$  has positive gain only in one segment  $s(\beta)$ , i.e., the one containing its main lobe. We call  $\mathcal{U}_{k,s} \subset \mathcal{U}_k$  the set of active users served by a beam whose main lobe is in segment  $s$ , i.e.,  $\mathcal{U}_{k,s} := \{u \in \mathcal{U}_k : s(\beta_{u,k}) = s\}$ . Then, the EIRP consumption  $c_{k,s}$  depends only on users  $\mathcal{U}_{k,s}$ :

$$c_{k,s} = \max_{(\phi, \theta) \in s} \sum_{u \in \mathcal{U}_{k,s}} A_{u,k} P_{u,k} G_{u,k}(\phi, \theta) \quad (7)$$

and the power allocation  $P_{u,k}$  for a user in  $\mathcal{U}_{k,s}$  does not impact the EIRP consumption over a different segment  $s' \neq s$ . In this case, we can optimize the user power allocation independently for each segment.

Next, computing  $c_{k,s}$  as in (7) requires the solution of an optimization problem. To circumvent it and simplify computations, we pre-compute the maximum gain for each beam:

$$\hat{G}_{u,k} := \max_{(\phi, \theta) \in s} G_{u,k}(\phi, \theta) \quad (8)$$

and we bound  $c_{k,s}$  via a simple-to-compute expression:

$$c_{k,s} \leq \sum_{u \in \mathcal{U}_{k,s}} A_{u,k} P_{u,k} \hat{G}_{u,k}. \quad (9)$$

Note that equality in (9) holds only if the gain is maximal in the same direction for all beams serving users in  $\mathcal{U}_{k,s}$ .

**Optimization problem.** We now formulate the problem of power allocation across UEs. For notation simplicity we drop the variable dependence on  $s, k$ , with the understanding that the same procedure is used at each slot  $k$  and segment  $s$ .

Let  $r_u(P_u)$  be the function mapping the power allocated to user  $u$  to its transmission rate per PRB. In practice,  $r_u$  is a staircase increasing function that can be well approximated as a continuous *concave* function, e.g.,  $r_u(P_u) = w \log(1 + P_u/N_u)$  where  $N_u$  is the noise plus interference PSD and  $w$  is an appropriate constant for the data channel codes used.

We allocate power across UEs by maximizing a fairness function of the UE throughput under the EIRP constraint. To this aim, we introduce the fairness function [12]:

$$f_\alpha(x) := \begin{cases} \frac{x^{1-\alpha}}{1-\alpha} & \text{if } \alpha \geq 0, \alpha \neq 1 \\ \log(x) & \text{if } \alpha = 1 \end{cases}. \quad (10)$$

and we formulate our power allocation problem for each segment  $s \in \mathcal{S}$  and slot  $k$  as follows:

$$\max_{\{P_u\}} \sum_{u \in \mathcal{U}} f_\alpha(A_u r_u(P_u)) \quad (11a)$$

$$\text{s.t.} \sum_{u \in \mathcal{U}} A_u P_u \hat{G}_u \leq b \quad (11b)$$

$$\underline{P}_u \leq P_u \leq \bar{P}_u, \quad \forall u \in \mathcal{U}. \quad (11c)$$

where in (11b) we used the consumption upper bound (9).

Note that, if  $\alpha = 1$ , then the objective function (11a) maximizes the proportional fairness of the throughput across UEs; as  $\alpha$  grows, it tends to max-min fairness [12]. The lower power value  $\underline{P}_{u,k}$  can be chosen such that reception is possible with the most robust modulation and coding scheme available.

**Water-filling solution.** Problem (11) is convex, with separable objective function and subject to linear constraints. Hence, if the feasibility region contains an interior point (known as Slater condition [13]), which holds if  $\underline{P}_u$ 's are sufficiently low, then Karush-Kuhn-Tucker (KKT) conditions are necessary and sufficient conditions for optimality [13]. In our case, KKT conditions lead to the following water-filling type solution.

Define the class of power allocations  $\{P_u^*(\nu)\}_u$ , depending on the value of a parameter (read, Lagrangian multiplier)  $\nu$ :

$$P_u^*(\nu) = \begin{cases} \bar{P}_u, & \text{if } (A_u \hat{G}_u)^{-1} \frac{d}{dP_u} f_\alpha(A_u r_u(\bar{P}_u)) > \nu \\ \underline{P}_u, & \text{if } (A_u \hat{G}_u)^{-1} \frac{d}{dP_u} f_\alpha(A_u r_u(\underline{P}_u)) < \nu \\ P^* : (A_u \hat{G}_u)^{-1} \frac{d}{dP_u} f_\alpha(A_u r_u(P^*)) = \nu, & \text{else} \end{cases} \quad (12)$$

Then, the solution to the problem (11) is  $P_u^* = P_u^*(\nu^*)$  for all UEs  $u$ , where  $\nu^*$  is the “water level” such that:

$$\nu^* = \max \left\{ \nu : \sum_u A_u \hat{G}_u P_u^*(\nu) \leq b \right\}. \quad (13)$$

Note that computing  $\nu^*$  in (13) requires one to find the root of the function  $\nu \rightarrow \sum_u A_u \hat{G}_u P_u^*(\nu) - b$ , which can be solved numerically via, e.g., the classic bisection method.

#### IV. SIMULATIONS

Our simulation experiments are performed in a DL system-level simulator implementing a 3GPP calibrated Urban Macro (UMa) [14] channel model, abstracting the physical-layer effects through a link to system-level interface computing equivalent Signal to Interference plus Noise Ratio (SINR) at transmission time, given the cell/user topology and the beamformed active transmissions in each cell. The simulation environment consists of a hexagonal deployment of seven three-sector sites at 500m inter-site distance, corresponding to 21 cells with gNB installed at 25m height and 12 degrees mechanical downtilt. The main simulation parameters can be found in Table I. The central frequency is at 3.5 GHz, with 273 PRBs at 30 kHz subcarrier spacing generating a 100 MHz carrier in Time Division Duplex (TDD) split, with an average ratio of 4 DL slots every uplink (UL) slot and a total simulation time of 12 seconds. In our considered massive MIMO scenario the gNBs is equipped with a uniform rectangular array of 192 cross-polarized antennas with 5.2 dBi gain. The UEs have 2 cross-polarized omni-directional antenna elements. The antenna spacing is defined in multiple of the wavelength  $\lambda$  in Table I. The wideband Channel Quality Indicator (CQI) report is provided every 160 ms to the gNB, with measurements taken every 80 ms. DL Beamforming is based on Sounding Reference Signal (SRS) transmitted by the UEs in UL, with beams selected among a codebook of Discrete Fourier Transform (DFT) beams [15] in the two-dimensional angular  $(\phi, \theta)$  plane. The UEs generate traffic according to the 3GPP File Transfer Protocol 2 (FTP2) traffic model [16], where each UE starts downloading a new packet of fixed dimension  $Q$  exactly 50 ms after its previous packet was successfully downloaded. The MAC scheduler architecture is depicted in Fig. 1. At most 8 UEs per slot according to proportional fair metrics in the “UE selection” block, and after the possible actions due to EIRP control, finally the available PRBs are allocated to them with a round robin criterion with single-user MIMO allocations for up to 4 layers. Matching the proportional-fair criterion, we chose  $\alpha = 1$  in (11) to maximize the geometric mean of throughput for the users connected the cell.

|                         |  |
|-------------------------|--|
| General Environment     | 3GPP UMa [14], no buildings                          |
| Cells deployment        | $7 \times 3$ sector sites at 500m distance           |
| Traffic model           | 210 FTP2 [16], Reading time 50 ms                    |
| CQI feedback            | Wideband reports every 160 ms                        |
| CQI/MCS Table           | CQI/MCS Table 2, 256 QAM [17]                        |
| Link Performance        | 3GPP data channel codes [17]                         |
| Central Frequency       | 3.5 GHz, TDD   |
| Subcarrier Spacing      | 30 kHz (0.5 ms slots)                                |
| Number of PRBs, band    | 273, 100 MHz   |
| Max Transmit Power, $P$ | 53 dBm, 0.73 W/PRB                                   |
| gNB Antennas, spacing   | 12x8 cross-pol, $0.7\lambda$ rows, $0.5\lambda$ cols |
| UE Antennas, spacing    | 2 cross-pol elements $0.5\lambda$                    |
| Spatial multiplexing    | Up to rank 4 Single User MIMO                        |
| User Mobility           | 3 km/h   |

TABLE I. MAIN SIMULATION PARAMETERS

A single segment is configured for the simulations to enforce a EIRP constraint over the whole sector  $\gamma^* = \rho\bar{\gamma}$ , where  $\bar{\gamma}$  is the maximum EIRP that can be radiated by the gNB array by using the full 53 dBm transmit power and maximum array gain at boresight, and the power reduction factor is  $0 < \rho \leq 1$ . The outer-loop algorithm curbing the long-term target is implemented according to [8]. The PL techniques described in Section III are compared against the “Resource Limiting (RL)” baseline used in [4], [5], where PRBs are consecutively allocated using  $P_{u,k} = \bar{P}$  to UEs in the slot as long as (9) is satisfied. The slot budget with “RL” and “PL” is computed with (5). The “PL - R” implements the budget refinement as per (6), with  $\rho^* = 0.1$  and  $b^* = 0.1\gamma^*$ . For reference, the curve without any EIRP control and power optimization [11] is plot with the “No EIRP Control” tag.

In Fig. 2 we compare the average throughput carried by each cell without EIRP limitation versus different EIRP enforcement techniques with  $\rho = 1/4$ . With “No EIRP Control”, we can observe how the carried load grows with increasing packet size  $Q$ , until the system saturation limit around 430 Mbits/s (black). Once activating EIRP control, a lower saturation point is to be expected. The RL technique (blue) saturates much earlier at 240 Mbits/s, but way above  $1/4$  of the system saturation limit, due to the average reduced interference. On the other hand, the PL techniques can be much closer to the system saturation limit, achieving up to 402 Mbits/s with the “PL - R” (red solid) and the hand-tuned  $\epsilon = 0.9$ . One can appreciate the small, but persistent gain of “PL - R” versus the simple “PL” (green), or the choice of less or more initial budget allocations in the period, with  $\epsilon = 1.0, 0.5$  (red dashed, dotted), respectively.

In Fig. 3 we plot the average throughput perceived by each UE, defined as the ratio between the bits successfully received versus the time the UE needs to receive them. Therefore, losses of UE throughput are observed with high packet size even without any EIRP limitation, due to the resource contention among UEs. In Fig. 3 we focus at just two EIRP control techniques, the best performing “PL - R” with  $\epsilon = 0.9$  (red) versus the RL baseline [4], [5]. Then, we compare their performance with increasing EIRP limitations with  $\rho = 1/2, 1/4, 1/8$  (cross, circle, plus markers), respectively. As expected, with lower  $\rho$  the UE throughput degrades with lower packet sizes, hence offered load. However, we can notice the improvements brought by “PL - R” technique, that are more consistent when the EIRP limit is more demanding. This is due by the superposition of two effects discussed in [10], [11]. First of all, the throughput loss scales logarithmically with the transmit power reduction. Moreover, the power optimization techniques [10], [11] applied by PL have the effect of stabilizing and reducing interference, resulting in the potentially higher peak performance, as also observed in Fig. 3 by the 5-8% gains at low loads, when comparing to the “No EIRP Control” baseline. Interestingly enough, with half of the maximum EIRP at  $\rho = 1/2$ , the UE throughput is reduced by less than 1% at mid-high loads with “PL - R”.

Finally, even if not shown for reason of space, we can

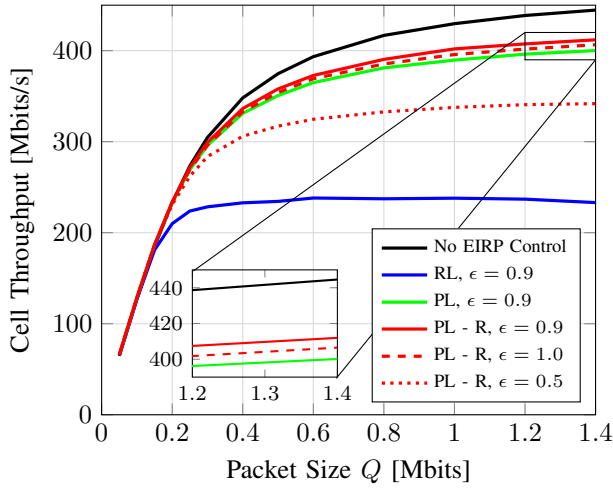


Fig. 2: Average throughput carried by each cell in the system with different EIRP control techniques at constant power reduction factor  $\rho = 1/4$  and the reference performance without any power adaptation and EIRP control.

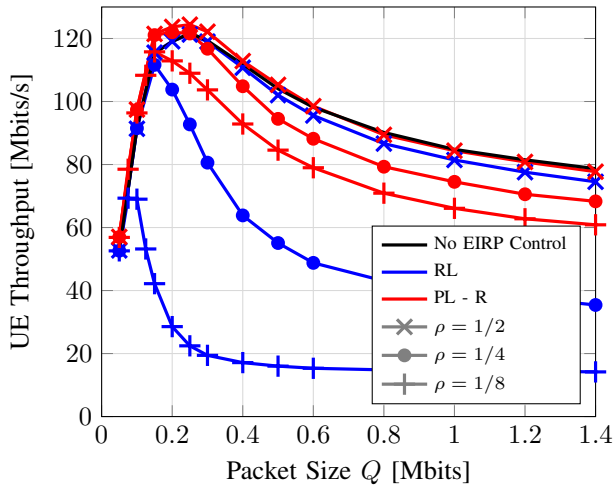


Fig. 3: Average UE throughput - defined as ratio between received bits and the time needed to receive them - without any power adaptation and EIRP control, for our best "PL - R" technique, and the baseline "RL", with different power reduction factors  $\rho$ .

confirm that all proposed EIRP control techniques discussed in this work were successful in enforcing the desired limitation.

## V. CONCLUSION

In this work we propose a family of techniques to spread the EIRP budget in each slot and then to allocate power and resources to UEs upon MAC scheduling slot-by-slot operations. Differently from MAC scheduling EIRP control prior art, we dynamically curb the power per UE in a computationally feasible manner. This is achieved by minimizing dependencies among different "segments" where EIRP constraints are active and by deriving a proper water-filling solution to the resulting parallel problems.

Our proposal allows to drastically reduce the communications performance losses compared to the legacy approaches

that dynamically adapt the resource allocation without any power adaptation. For example, in case of 25% allowed EIRP, our best proposal loses only 6.5% in cell throughput, in contrast to the 44.2% reduction with the legacy approaches. The minimal computational overhead and the performance achieved in our extremely detailed simulation study confirm that our technique is a standout candidate to enforce EIRP constraints in slot-by-slot operations of 5G and future 6G MAC schedulers.

## ACKNOWLEDGEMENTS

The authors would like to thank Tedros Abdu for the great discussions and feedback during the evolution of this study.

## REFERENCES

- [1] I. C. on Non-Ionizing Radiation Protection (ICNIRP), "Guidelines for limiting exposure to electromagnetic fields (100 kHz to 300 GHz)," *Health physics*, vol. 118, no. 5, pp. 483–524, 2020.
- [2] K. Karipidis, R. Mate, D. Urban, R. Tinker, and A. Wood, "5G mobile networks and health—A state-of-the-science review of the research into low-level RF fields above 6 GHz," *Journal of Exposure Science & Environmental Epidemiology*, vol. 31, no. 4, pp. 585–605, 2021.
- [3] S. Wesemann, J. Du, and H. Viswanathan, "Energy efficient extreme MIMO: Design goals and directions," *IEEE Communications Magazine*, 2023.
- [4] C. Törnevik, T. Wigren, S. Guo, and K. Huisman, "Time averaged power control of a 4G or a 5G radio base station for RF EMF compliance," *IEEE Access*, vol. 8, pp. 211 937–211 950, 2020.
- [5] T. Wigren and C. Törnevik, "Coordinated average EIRP control of radio transmitters for EMF exclusion zone computation," *IEEE Wireless Communications Letters*, vol. 10, no. 9, pp. 2075–2079, 2021.
- [6] M. R. Castellanos, D. J. Love, and B. M. Hochwald, "Hybrid precoding for millimeter wave systems with a constraint on user electromagnetic radiation exposure," in *2016 50th Asilomar Conference on Signals, Systems and Computers*. IEEE, 2016, pp. 296–300.
- [7] P. Baracca, A. Weber, T. Wild, and C. Grangeat, "A statistical approach for RF exposure compliance boundary assessment in massive MIMO systems," in *WSA 2018; 22nd International ITG Workshop on Smart Antennas*. VDE, 2018, pp. 1–6.
- [8] L. Maggi, A. Herzog, C. Grangeat, and A. Zejnilagic, "Smooth power control for EMF compliance with minimum traffic guarantees," to appear soon in *ArXiv*, 2024.
- [9] P. Kela, J. Puttonen, N. Kolehmainen, T. Ristaniemi, T. Henttonen, and M. Moisio, "Dynamic packet scheduling performance in UTRA long term evolution downlink," in *2008 3rd International Symposium on Wireless Pervasive Computing*. IEEE, 2008, pp. 308–313.
- [10] S. Mandelli, A. Lieto, P. Baracca, A. Weber, and T. Wild, "Power optimization for low interference and throughput enhancement for 5G and 6G systems," in *2021 IEEE Wireless Communications and Networking Conference Workshops (WCNCW)*. IEEE, 2021, pp. 1–7.
- [11] S. Mandelli, A. Lieto, M. Razenberg, A. Weber, and T. Wild, "Reducing interference via link adaptation in delay-critical wireless networks," *EURASIP Journal on Wireless Communications and Networking*, vol. 2022, no. 1, p. 109, 2022.
- [12] J. Mo and J. Walrand, "Fair end-to-end window-based congestion control," *IEEE/ACM Transactions on networking*, vol. 8, no. 5, pp. 556–567, 2000.
- [13] S. P. Boyd and L. Vandenberghe, *Convex optimization*. Cambridge university press, 2004.
- [14] 3GPP, "TR 38.901. Study on channel model for frequencies from 0.5 to 100 GHz," Technical Report, 2023.
- [15] M. D. Zoltowski, M. Haardt, and C. P. Mathews, "Closed-form 2-D angle estimation with rectangular arrays in element space or beamspace via unitary ESPRIT," *IEEE Transactions on Signal Processing*, vol. 44, no. 2, pp. 316–328, Feb. 1996.
- [16] 3GPP, "TR 36.814. Further advancements for E-UTRA physical layer aspects," Technical Report, 2017.
- [17] —, "TS38.214. NR; Physical layer procedures for data," Technical Specification, 2020.